

1 **Samples description:**

2 110 peridotites have been collected from three sites within the Natron lake magmatic province
3 (<10 km from OL; N-Tanzania) in the East African Rift: Pelo Hill, Eledoi, and Oldoinyo
4 Lengai. Xenoliths correspond to round to subangular blocks of spinel lherzolites,
5 harzburgites, wherlites and dunites. Xenoliths are embedded in silicate host lavas that only
6 contain carbonates locally, those display the same petrographic details than those of the
7 xenoliths. The silicate host lavas contain clinopyroxene ($\approx 100\mu\text{m}$), nepheline ($\approx 200\mu\text{m}$),
8 melilite ($\approx 100\mu\text{m}$) and perovskite ($\approx 200\mu\text{m}$) as the main phenocryst phases. Carbonates are
9 present as sub-euhedral grains (<1mm). Olivine and clinopyroxene xenocrysts, originating
10 from the mantle xenoliths, have also been observed. Following the classification of [Mercier](#)
11 [and Nicolas \(1975\)](#), xenoliths textures vary from protogranular to porphyroclastic. In
12 protogranular-textured rocks, the grain-size of olivine is bimodal with fine-grained domains
13 (<1 mm), and coarse-grained domains (20 mm); 120° triple junctions are common. Unlike the
14 small olivines, large olivine grains and orthopyroxenes often show undulated extinctions.
15 Clinopyroxenes are anhedral diopside, and contain up to 4.5 % wt Cr_2O_3 (acquired by EPMA
16 at SCMEM, Nancy) casting for a metasomatic origin ([O'Reilly and Griffin, 1988](#)). A marked
17 hydrous metasomatic stage is also recorded by both intergranular grains and veins of
18 amphibole and/or phlogopite, consistent with previous studies of the regional mantle (e.g.
19 [Dawson and Smith, 1988](#)). Distinctive diopside-spinel-amphibole and/or phlogopite
20 porphyroclastic aggregates are up to 6 mm. Hydrous minerals are free of any kind of textural
21 deformation. Among the samples studied here, ten host carbonate phases. The present study
22 focuses on three of those samples selected for their representativity, as well as on two samples
23 from the study of [Lee et al. \(2000\)](#), collected in the same area at Eledoi and Monduli.

24

Carbonates were observed in all mantle lithologies (lherzolite, wherlite, harzburgite, and dunite), whether the samples were strongly metasomatized or free of any metasomatic evidence. Carbonates were analysed in xenoliths: EL14: a spinel dunite (Eledoi), 24A4: a spinel lherzolite (Eledoi), 24C4: a phlogopite spinel wherlite (Eledoi), 19B: a phlogopite spinel dunite (Pelo Hill), and MON5: a spinel harzburgite (Monduli). EL14 and MON5 were also studied by [Lee et al. \(2000\)](#).

Thin sections are scattered with round holes that may have been occupied by carbonates or other inclusion types before preparation. Carbonate veins contain microcrystalline carbonates following grain boundaries and filling fractures. They are generally connected to the external surface of the xenolith. Carbonates in the host lava are typically present as patches of microcrystalline and discrete sub-euhedral grains (<1mm).

The analysed carbonates are calcite, ranging from $\#Ca=Ca/(Ca + Mg + Fe)$ in molar proportion of 0.85 to pure calcite (Table S2). This range encompasses the calcite chemistry previously observed at these sites (from 0.93 to pure calcite, [Lee et al., 2000](#)) and the calcites in metasomatic veins in mantle xenoliths from Eledoi from [Mattsson et al., 2013](#).

Carbon isotopes measurements:

The carbon coating of the sample was removed by polishing after SEM and EPMA analysis to avoid carbon contamination during the C-isotope measurements. Moreover, a presputtering of 90s with a raster of 20x20 μm was included in the routine of analysis in order to remove remaining traces of the carbon coating. Then, the sample was coated by a gold film of ≈ 30 nm thick. Carbon isotopes analyses were performed using a CAMECA IMS 1270 E7 ion microprobe at the CRPG-CNRS (Nancy, France). A Cs^+ primary Gaussian beam of 4 nA accelerated at 10 kV was focused to a 15 μm wide spot. A normal-incidence electron gun was used for charge compensation. Entrance and exit slits were set to obtain a mass resolving power (MRP, $M/\Delta M$) of 5000 in order to eliminate the $^{12}\text{CH}^+$ contribution to ^{13}C (slit 2; Rollion-Bard *et al.*, 2007). Measurements of carbon isotopes were conducted in multicollection mode using one off-axis faraday cups (L'2) with 10^{11} ohm resistors for ^{12}C and one electron multiplier (EM) for ^{13}C . A pure calcite (Table S2) was used as standard to compensate the matrix effects caused by the samples chemistry and to correct the instrumental mass fractionation (IMF). The typical counting rate of $^{12}\text{C}^-$ was 2×10^7 cps, and 2×10^5 cps for $^{13}\text{C}^-$. The acquisition times were 5 sec repeated over 40 cycles. Automatic centering of the transfer deflectors and mass was implemented in the analysis routine to minimize IMF variations. Doing this, the typical internal error for each measurement was $\approx 0.30\text{‰}$ (2σ), and the external reproducibility on the calcite standard was around 0.30‰. Results are expressed in the usual per mil notation relative to the Pee Dee Belemnite (PDB) marine carbonate reference material.

Oxygen isotopes measurements:

The carbon coating of the sample was removed after SEM and EPMA analysis. Moreover, a presputtering of 90s with a raster of 20x20 μm was included in the routine of analysis in order to remove remaining traces of the carbon coating. We measured oxygen isotopic compositions with a CAMECA IMS 1270 E7 at CRPG-CNRS (Nancy, France). A Cs^+ primary Gaussian beam of 4 nA accelerated at 10 kV was focused to produce a spot of 15 μm wide. Charge accumulations on the sample surface were neutralized by the use of a normal-incidence electron gun. The mass spectrometer entrance slit was 150 mm, the field aperture was 2000 μm and the multicollection slit was 500 mm (slit 1). This tuning results in a mass resolving power ($M/\Delta M$) of 2500. Under these conditions, the interferences of $^{16}\text{OH}_2^-$, $^{17}\text{OH}^-$ and $^{16}\text{OD}^-$ peaks are completely resolved from the corresponding oxygen isotopes. Automatic centering of the transfer deflectors and mass was implemented in the analysis routine. Ions were measured in multicollection mode using three faraday cups L'2 ($^{16}\text{O}^-$) and H1 ($^{18}\text{O}^-$). A pure calcite and an ankerite were used as standards to determine the instrumental mass fractionation (IMF) due to matrix effects. The typical counting rate of $^{16}\text{O}^-$ was 3×10^9 cps, and 7×10^6 cps for $^{18}\text{O}^-$ on the calcite and ankerite standards. The acquisition times were 5 sec repeated over 30 cycles. Doing this, the typical internal error for each measurement was $\approx 0.15\text{‰}$ (2σ) on $\delta^{18}\text{O}$ and the external reproducibility was around 0.20‰ on both standards. Results are expressed in the usual per mil notation relative to the Standard Mean Ocean Water (SMOW) marine carbonate reference material. $\delta^{18}\text{O}$ values were corrected using Carb CRB calcite standard but, because of the presence of MgO in the samples but not in the calcite standard, Rollion-Bard et al. (2011) showed that an error of $\approx 2\text{‰}$ on the IMF could occur. However, these uncertainties do not affect the established discussion on the data.

Rayleigh distillation model

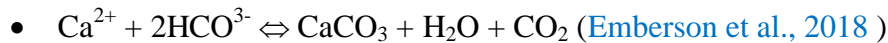
On fig.3, the field labeled “OL” defines the C-O isotopic compositions of fresh natrocarbonatites from Oldoinyo Lengai (Keller & Zaitsev, 2006) ($\delta^{18}\text{O} = ((^{18}\text{O}/^{16}\text{O})_{\text{sample}} / (^{18}\text{O}/^{16}\text{O})_{\text{standard}}) - 1) * 1000$; $\delta^{13}\text{C} = ((^{13}\text{C}/^{12}\text{C})_{\text{sample}} / (^{13}\text{C}/^{12}\text{C})_{\text{standard}}) - 1) * 1000$); alt.OL represents altered Oldoinyo Lengai natrocarbonatites (Keller & Hoefs, 1995). The field labeled “Mantle” is based on C isotopic compositions of oceanic basalts (Kyser, 1986; Nelson et al., 1988; Deines, 1989) and O isotopic compositions of mantle xenoliths (Mattey et al., 1994). The “Carbonatites” field is from Hay (1989) and Keller & Hoefs (1995). The Rayleigh Distillation Model (RDM) is calculated at 15 and 35 °C, using an initial $\delta^{18}\text{O} = -2 \pm 2\text{‰}$ for rainfall (Bowen, 2010; Otte et al., 2017), an initial $\delta^{13}\text{C}$ value of -25‰ for dissolved inorganic carbon in the case of C3 plants, and an initial $\delta^{13}\text{C}$ value of -15‰ for in the case of C4 plants (Yoneyama et al., 2010); Mg matrix effect: $\delta^{18}\text{O}$ values were corrected using a calcite standard; the low Mg content of carbonates may induce a slight instrumental mass fractionation that would affect the data by less than 2‰ (Rollion-Bard et al., 2011).

$\delta^{18}\text{O}$ fractionation during carbonate precipitation was calculated using:

$$\bullet \quad \delta^{18}\text{O}: 1000\ln(\alpha_{\text{calcite-fluid}}) = 18.03(10^3/T) - 32.42 = \Delta_{\text{calcite-fluid}}$$

$$\bullet \quad \text{with } \Delta_{\text{calcite-fluid}} = \delta^{18}\text{O}_{\text{calcite}} - \delta^{18}\text{O}_{\text{fluid}} \text{ (Kim and O'Neill, 1997)}$$

$\delta^{13}\text{C}$ fractionation during the Rayleigh distillation was based on the equation:



Accounting for the precipitation of calcite associated with CO_2 degassing, and using a temperature-dependent isotopic fractionation factor of 0.9946 at 15 °C and 0.9955 at 35 °C (e.g., Embersson et al., 2018).

$\delta^{13}\text{C}$ fractionation was calculated using:

$$\bullet \quad \delta^{13}\text{C}_B = \delta^{13}\text{C}_{\text{initial}} + 1000 * (f(\alpha_{B-A} - 1) - 1)$$

$$\text{with } f = \text{water fraction; } \alpha_{B-A} = (1000 + \delta^{13}\text{C}_B) / (1000 + \delta^{13}\text{C}_A); \text{ A = water; B = Calcite.}$$

References

- Bowen, G.J., 2010, Isoscapes: Spatial Pattern in Isotopic Biogeochemistry: Annual Review of Earth and Planetary Sciences, v. 38, p. 161–187.
- Dawson, J.B. and Smith, J.V., 1988, Metasomatised and veined upper-mantle xenoliths from Pello Hill, Tanzania: evidence for anomalously-light mantle beneath the of the East African Rift Valley Tanzanian sector: Contributions to Mineralogy and Petrology, v 100, p. 510-527.
- Dawson, J. B., 1992, Neogene tectonics and volcanicity in the North Tanzania sector of the Gregory Rift Valley: contrasts with the Kenya sector: Tectonophysics, v 204(1-2), p. 81-92.
- Deines P., 1989, Stable isotope variations in carbonatites. In: Bell K (ed) Carbonatites - genesis and evolution. Unwin Hyman, London, p 301-359.
- Emberson, R., Galy, A., and Hovius, N., 2018, Weathering of reactive mineral phases in landslides acts as a source of carbon dioxide in mountain belts: Journal of Geophysical Research: EarthSurface, v. 123, p. 2695–2713.
- Hay, R.L., 1989, Holocene carbonatite-nephelinite tephra deposits of Oldoinyo Lengai, Tanzania: Journal of Volcanology and Geothermal Research, v 37, p 77-91.
- Keller, J., and Hoefs, J., 1995, Stable isotope characteristics of recent natrocarbonatites from Oldoinyo Lengai: Lithos, v. 91, p. 150–172.
- Keller, J., & Zaitsev, A. N., 2006, Calciocarbonatite dykes at Oldoinyo Lengai, Tanzania: the fate of natrocarbonatite: The Canadian Mineralogist, v 44(4), p 857-876.

141 Kim, S.T., and O'Neill, J.R., 1997, Equilibrium and nonequilibrium oxygen isotope effects in
142 synthetic carbonates: *Geochimica et Cosmochimica Acta*, v. 61, p. 3461–3475.

143 Kyser TK., 1986, Stable isotope variations in the mantle. In: Valley JW et al. (eds) *Stable*
144 *Isotopes in high temperature geological processes. Reviews in Mineralogy and*
145 *Geochemistry*, v 16, p 141-164.

146 Lee, C-T., Rudnick, R.L., McDonough, W.F. and Horn, I., 2000, Petrologic and geochemical
147 investigation of carbonates in peridotite xenoliths from northeastern Tanzania:
148 *Contributions to Mineralogy and Petrology*, v 139, p. 470-484.

149 Mattsson, H. B., Nandedkar, R. H., and Ulmer, P., 2013, Petrogenesis of the melilititic and
150 nephelinitic rock suites in the Lake Natron–Engaruka monogenetic volcanic field, northern
151 Tanzania: *Lithos*, v 179, p. 175-192.

152 Matthey, D., Lowry, D., and Macpherson, C., 1994, Oxygen isotope composition of mantle
153 peridotite: *Earth Planet. Earth and Planetary Science Letters*, v. 128, p. 231–241.

154 Mercier, J-C.C. and Nicolas, A., 1975, Textures and Fabrics of Upper-Mantle Peridotites as
155 Illustrated by Xenoliths from Basalts: *Journal of Petrology*, v 16, p. 454.

156 Nelson, D.R., Chivas, A.R., Chappell, B.W. and McCulloch, M.T., 1988, Geochemical and
157 isotopic systematics in carbonatites and implications for the evolution of ocean-island
158 sources: *Geochimica et Cosmochimica Acta*, v 52, p 1-17.

159 Otte, I., Detsch, F., Gütlein, A., Scholl, M., Kiese, R., Appelhans, T., and Nauss, T., 2017,
160 Seasonality of stable isotope composition of atmospheric water input at the southern slopes
161 of Mt. Kilimanjaro, Tanzania: *Hydrological Processes*, v. 31, p. 3932–3947.

162 O'Reilly, S.Y. and Griffin, W.L., 1988, Mantle metasomatism beneath western Victoria,
 163 Australia: 1. Metasomatic processes in Crdiopside lherzolites: *Geochimica et*
 164 *Cosmochimica Acta*, v 52, p. 433-447.

165 Rollion-Bard, C., Mangin, D. and Champenois, M., 2007, Development and application of
 166 oxygen and carbon isotopic measurements of biogenic carbonates by ion microprobe:
 167 *Geostandards and Geoanalytical Research*, v 31, p. 39-50.

168 Rollion-Bard, C. and Marin-Carbonne, J., 2011, Determination of SIMS matrix effects on
 169 oxygen isotopic compositions in carbonates: *Journal of Analytical Atomic Spectrometry*, v
 170 26, p. 1285-1289.

171 Yoneyama, T., Okada, H., and Ando S., 2010, Seasonal variations in natural ^{13}C abundances
 172 in C_3 and C_4 plants collected in Thailand and the Philippines *Soil: Science and Plant*
 173 *Nutrition*, v. 56, p. 422–426.

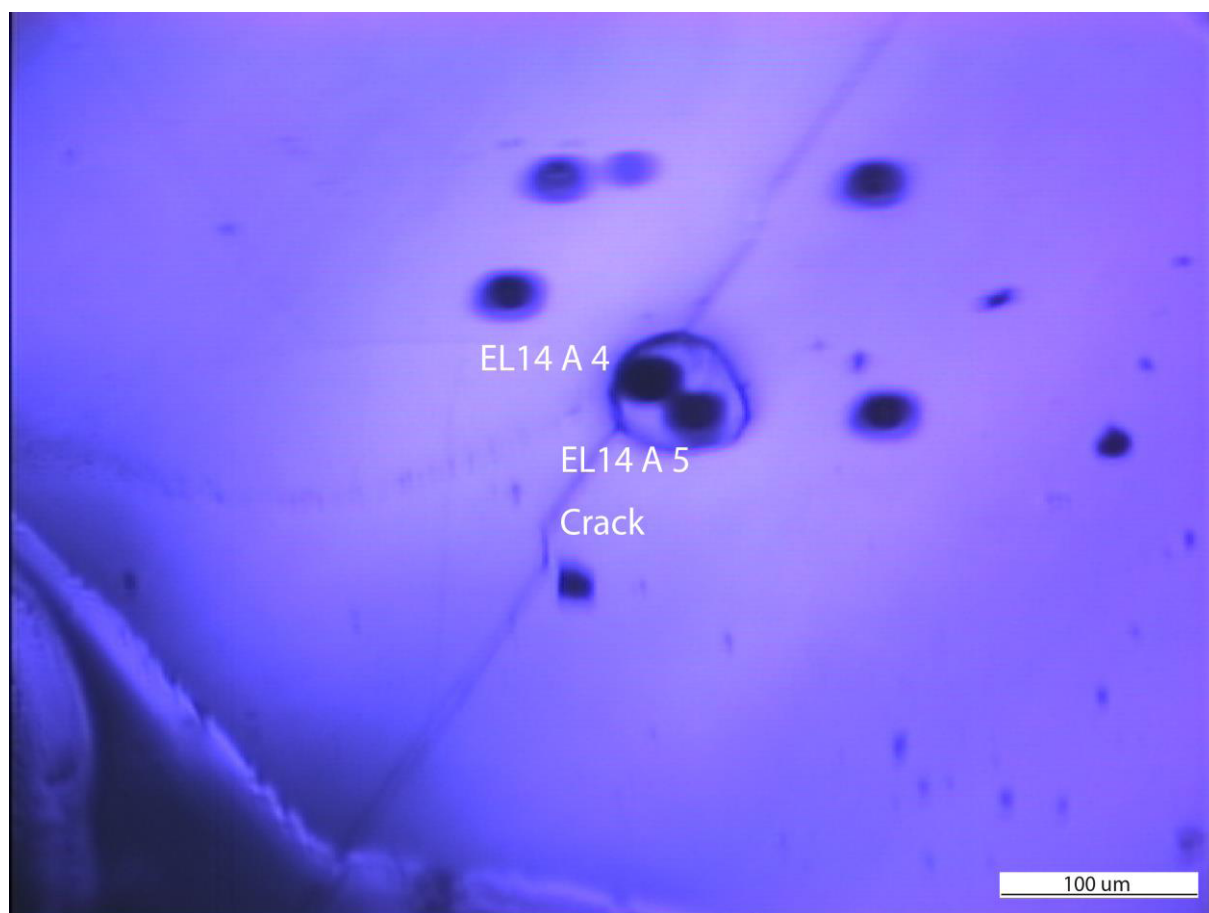
Supplementary material:



Casola et al., Figure S1

Typical maar related pyroclastic deposit in the Natron Lake magmatic province displaying melilitite juvenile material (light grey ash and lapilli), mantle xenoliths (green to yellow material), free phlogopite crystals (red circle), and pedogenic carbonates invading the area of the outcrop (white background). Picture is taken at Embalulu Oltatwa maar on Oldoinyo Lengai Eastern flank.

Carbonate description:



Casola et al., Figure S2

Several carbonate inclusions in this study contain two $\delta^{18}\text{O}$ analysis spots to which are associated several $\delta^{13}\text{C}$ analyses (Fig. S2, Table S1). The letters correspond to the inclusion name and the associated last number refers to the SIMS spots in the inclusion. For example EL14 A 4 and EL14 A 5 means that the inclusion A in EL14 contains two spots (named 4 and 5) to which several $\delta^{13}\text{C}$ analyses are associated.



Casola et al., Fig. S3

Location map of the studied area (*Google Earth*). The red dots refer to the samples obtained at Pelo Hill and Eledoi.